REPORT DOCUMENTATION PAGE

Form Approved
OMB No. 0704-0188

1. AGENCY USE ONLY *(Leave blank)*	2. REPORT DATE March 29, 2004	3. REPORT TYPE AND DATES COVERED *Dec 30,* FinalReport – Sept 15, 2000-~~9/14~~/2003

4. TITLE AND SUBTITLE
A Next Generation Scalable Finite Element Software to Describe Fracture and Fragmentation of Solids and Structures

5. FUNDING NUMBERS
DAAD19-00-1-0546

6. AUTHOR(S)
J. Knap, A. Mota and M. Ortiz (PI)

7. PERFORMING ORGANIZATION NAME(S) AND ADDRESS(ES)
Caltech
1200 E. California Blvd/MS 105-50
Pasadena, CA 91125

8. PERFORMING ORGANIZATION REPORT NUMBER
~~MO2.00004 1 ARO.000013~~

9. SPONSORING / MONITORING AGENCY NAME(S) AND ADDRESS(ES)
Army Research Office
Attn: AMSRD-ARL-RO-DS
PO Box 12211
Research Triangle Park, NC 27709-2211

20040405 072

41630.1-EG

11. SUPPLEMENTARY NOTES

12a. DISTRIBUTION / AVAILABILITY STATEMENT
Approved for Public Release; distribution unlimited

12b. DISTRIBUTION CODE

13. ABSTRACT *(Maximum 200 words)*

1 Summary of accomplishments

The overarching goal of the originally proposed work was the development of a new generation scalable Lagrangian finite element software framework capable of capturing local and non-local fracture processes in solids and structures. The principal objectives of the work, as stated in the proposal, were:
1. Development a scalable Lagrangian software framework to simulate fracture and fragmentation due to weapon-target interactions.
2. Implementation of complex phenomenological as well as physics-based advanced material strength and damage models.
3. Validation and verification of software through simulation of several benchmark DoD application problems
All the objectives have been successfully achieved. Some of the main developments are summarized in the text.

14. SUBJECT TERMS

15. NUMBER OF PAGES
10

16. PRICE CODE

17. SECURITY CLASSIFICATION OF REPORT	18. SECURITY CLASSIFICATION OF THIS PAGE	19. SECURITY CLASSIFICATION OF ABSTRACT	20. LIMITATION OF ABSTRACT

A Next Generation Scalable Finite Element Software to Describe Fracture and Fragmentation of Solids and Structures

J. Knap, A. Mota and M. Ortiz (PI)
Graduate Aeronautical Laboratories
California Institute of Technology
Pasadena, CA 01125

1   Summary of accomplishments

The overarching goal of the originally proposed work was the development of a new generation scalable Lagrangian finite element software framework capable of capturing local and non-local fracture processes in solids and structures. The principal objectives of the work, as stated in the proposal, were:

1. Development a scalable Lagrangian software framework to simulate fracture and fragmentation due to weapon-target interactions.

2. Implementation of complex phenomenological as well as physics-based advanced material strength and damage models.

3. Validation and verification of software through simulation of several benchmark DoD application problems

All the objectives have been successfully achieved. Some of the main developments are summarized in the text.

2   The scalable Lagrangian finite element software framework

Over the past decade, the PI has developed state-of-the-art Lagrangian finite element (FE) software capable of simulating crack initiation and growth in solids and structures. The software, written 'in high-level languages (Fortran, C and C++), was designed to

1

execute reliably in uni-processor computing environments (personal computers, work-stations, etc.). In addition, over the years, it underwent thorough testing and performance tuning. Therefore, this serial software become a suitable candidate to be turned into a core of the parallel FE framework.

Our parallel implementation was based on a dynamic decomposition of the computational domain among the processor with standard partitioning techniques (METIS). A two level approach was adopted in order to achieve scalability in the distributed computing environments. Initially, a set of multi-threaded (MT) extensions to the serial software was developed as to provide for the optimal performance on symmetric multi-processors (SMP). Subsequently, the implementation was amended by the addition of extensions based on the standard message passing interface (MPI), designed to allow for the distribution of simultaneous computational tasks across heterogenous parallel computing environments. This two tier approach lead to exceptional scalability and performance (Figure 1).
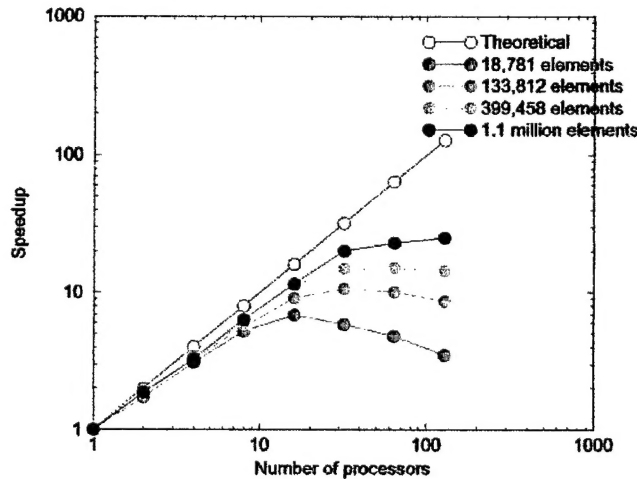

Figure 1: Measured speedup of the parallel software framework for the varying problem size.

In the design process, we decided to consider the use of commercial products for the pre- and post-processing. To this end we developed an interface for the FEMAP neutral file format as the model input. FEMAP is a popular engineering FE analysis package that supports solid modeling, FE model generation and post-processing. In addition, FEMAP offers the ability to import pre-existing FE models in many CAD file formats. In an attempt to allow the end-user to create high-quality visualizations, an interface for the output in TECPLOT visualization toolkit file format was also built.

The material library is an integral and essential part of the parallel FE framework. In order to facilitate the reuse or exchange existing material models, in particular those models that had been implemented in other DoD software, the strict material interface guidelines (MIG) were established and followed. This MIG format allowed the

US Army Research Laboratory (ARL) personnel to successfully import the material models implemented in other FE software (e.g. EPIC).

The software development required close collaboration between both the Caltech and the ARL teams. In order to simplify the process a CVS source repository was set up, with the ARL team having full access to the parallel framework source code through out the entire course of the project.

3   Parallel fracture algorithm

Many engineering problems involving fracture and fragmentation phenomena cannot be addressed on serial and vector computers due to processing time or storage requirements. However, in the context of MPI-based domain decomposition algorithm, a simple extension of the serial fracture and fragmentation approach is not feasible. Therefore, as an initial step towards the scalable fully three-dimensional (3D) fracture and fragmentation software implementation, a considerably simpler, two-dimensional (2D) version was developed. On the basis of this effort, we adopted an approach based on the introduction of cohesive elements in the FE discretization directly in the vicinity of all processor boundaries at the onset of the simulation. This approach significantly reduced the complexity of the 3D fracture and fragmentation software module, as well as decreased the development time. In addition, the 3D implementation was designed as easily expandable as to allow to incorporate other models of physical behavior that requires topological changes in the FE discretizations (e.g. adiabatic shear bands).

4   Adiabatic shear-band modeling

Solids deforming at high rates often develop narrow layers of intense shearing. Outstanding features of these dynamic shear bands are their thinness, high local shear strains, ultra-high local shear strain rates, significant local temperature rises and high propagation speeds. When simulating shear-bands, the commonly adopted approach calls for mesh adaption to resolve the fine scales in the solution. This, in turn, may significantly increase the size of the FE problem, placing more demands in terms of computer power or storage. An alternative approach is to employ a special type of finite elements, which serve the purpose of capturing sub-grid localization processes such as shear bands and void sheets[8]. These elements consist of two surfaces, attached to the abutting volume elements, which can separate and slip relative to each other. The kinematics of the strain-localization elements is three-dimensional and allows for finite deformations. The behavior of the strain-localization elements is governed directly by the same constitutive relation which describes the deformation of the volume elements. In particular the localization elements allow for the development of displacement and velocity jumps across volume element boundaries. The thickness of the localized zone is set by an additional field variable which is determined variationally. The localization elements are inserted, and become active, only when localized deformations become energetically favorable.

3

5 Tetrahedral composite finite elements

The quadratic tetrahedral elements have been know to under-perform in explicit time integration and contact-impact problems, due to the corner node masses being negative or zero. Thoutireddy *et al.*[6] introduced a composite 'CT3D' tetrahedral element that overcomes the difficulties inherent to the quadratic elements, making it perfectly suited for impact problems. The composite tetrahedron consists of an ensemble of 12 four-node linear tetrahedral elements, coupled to a linear assumed deformation defined over the entire domain of the composite element. The formulation of the element accounts for fully non-linear kinematics. Integrals over the domain of the element are computed by a five-point quadrature rule. The element passes the patch test in arbitrarily distorted configurations. Numerical tests demonstrate that CT element has been found to possess a convergence rate comparable to those of linear simplicial elements, and that these convergence rates are maintained as the near-incompressible limit is approached.

6 Validation tests

We have validated the new three-dimensional parallel capability by means of extensive comparison with archival data. Some relevant work in this direction is the following:

6.1 Three-dimensional modeling of dynamic mixed-mode fracture

As the first validation case, we have taken the dynamic mixed-mode fracture as a convenient basis for assessing the predictive ability of cohesive models in applications that involve competition between crack initiation and growth [5]. The predictions of our numerical model are validated against the experimental data of John and Shah [4]. These tests were concerned with three-point-bend beam (TPB) plain concrete specimens containing a pre-crack shifted from the central cross-section. The location of the pre-crack was characterized by the relative offset $\gamma = 2\text{offset}/L$, where L was the length of the beam. The presence of the pre-crack led to asymmetric loading conditions and resulted in mixed-mode fracture. Specimens were tested dynamically by means of a modified Charpy tester. By increasing its offset, the pre-crack was subjected to increasingly mode-II fracture conditions, and the trajectory of the crack varied accordingly. In addition, the experimental data is indicative of a competition between two fracture mechanisms: the growth of the pre-crack; and the nucleation and subsequent growth of a crack within the central cross-section of the specimen. The fracture behavior of the specimen was also observed to be sensitively dependent on the rate of loading.

Figure 3 displays computed crack patterns for relative offsets $\gamma = 0.6, 0.7$ and 0.8, respectively, and thus illustrates the dependence of the predicted failure mode on the location of the notch. In the experiments of John as Shah [4] a change in failure mode from pre-notch extension to crack nucleation within the plane of the load was observed at a critical offset of $\gamma = 0.7$. Our calculations are in very good agreement with the experimental observations, as the computed critical γ is identical to its experimental counterpart. Moreover, our results show that the model is indeed capable of closely
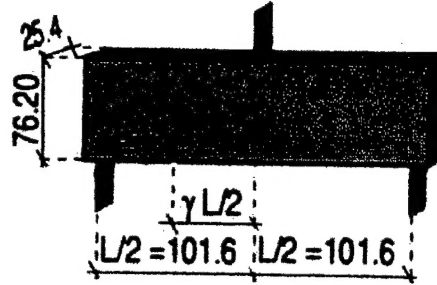
4

Figure 2: The three-point-bend beam configuration of John and Shah [4] (dimensions in mm).

capturing the observed fracture patterns, crack trajectories and crack-tip displacement fields corresponding to different experimental configurations. In particular, it correctly accounts for the relative stability regimes of the competing pre-crack growth vs. crack nucleation mechanisms.

6.2 Ring expansion and fragmentation

The second validation case concerns the simulation of forced expansion and ductile fracture and fragmentation of U-6%Nb rings [7, 1]. A sample ring expands driven by a driver ring under the magnetic field induced by the electric current applied to a solenoid. The ring has an inner diameter of 34.37 mm, an outer diameter of 35.89 mm, and thickness of 0.76 mm. An arrestor ledge in the experimental device prevents the driver ring to expand beyond a diameter of 40.0 mm. In contrast, the sample ring can expand freely, until it eventually fragments. The initial velocity history applied to the U-6%Nb ring varies according to the three different accelerating voltages of 5.0 kV, 6.0 kV, and 7.5 kV [1, 3]..

The U-6%Nb alloy is assumed to obey the porous plasticity model due to Weinberg *et al.* [7], with the strain localization part of Yang *et al.* [8]. Figure 4 shows the finite element discretization employed in our calculations. The initial number of nodes is 2,634 and the number of elements is 882. The nucleation and propagation of fracture is simulated by adaptively inserting strain localization elements when the accumulated plastic strain in the bulk elements reaches the value of 0.4.

The experimental velocity histories reported by Becker [1], as well as those obtained in our simulations, are shown in Figure 5. In order to simulate the effect of the driver ring, the radial velocity of all the nodes located on the inner radius is initially prescribed to match the radial velocity of the driver ring, as measured in the experiment, up to the peak velocity for each curve in Figure 5. A noticeable decrease in the ring velocity may be observed, a clear symptom of the kinetic energy being converted into the work of plastic deformation. This regime is subsequently followed by a plateau, indicative of ring fragmentation. Clearly, our calculations are capable of capturing the onset of the plastic flow, as well as, the initiation of fracture and fragmentation.
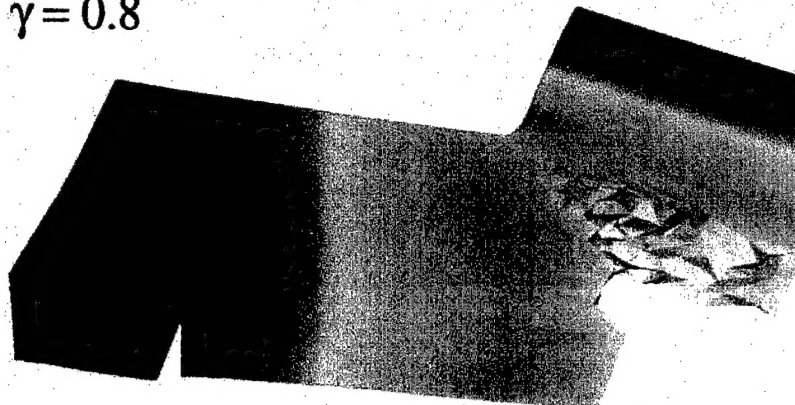
5

γ = 0.6

γ = 0.7
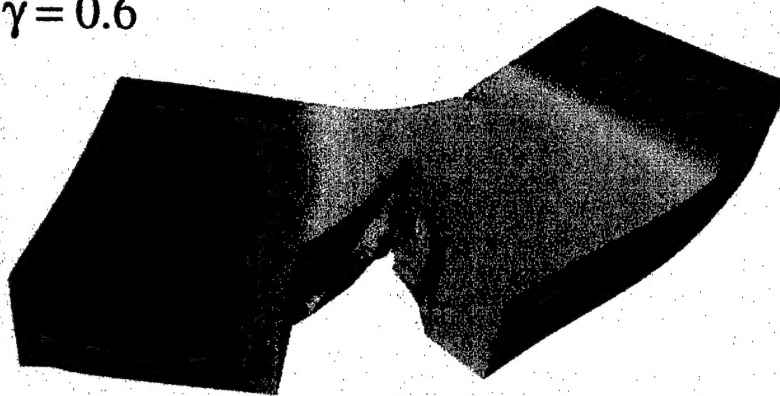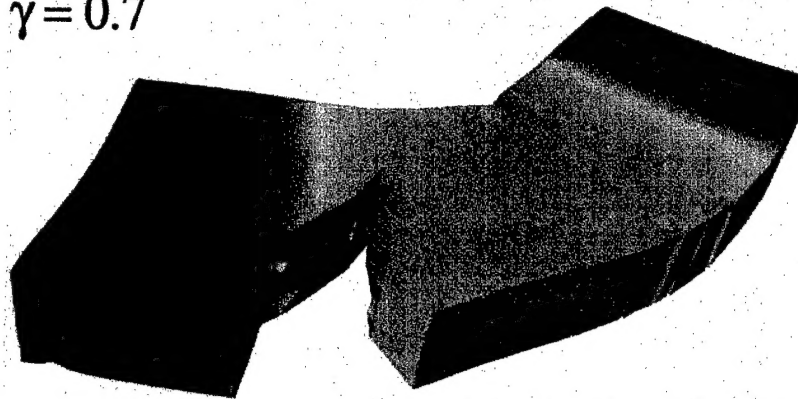
γ = 0.8

Figure 3: Numerical simulations of the three-point-bend experiments of John and Shah [4]. Effect of the pre-notch offset on crack pattern and failure mode. The color coding corresponds to the magnitude of the vertical displacement.

6

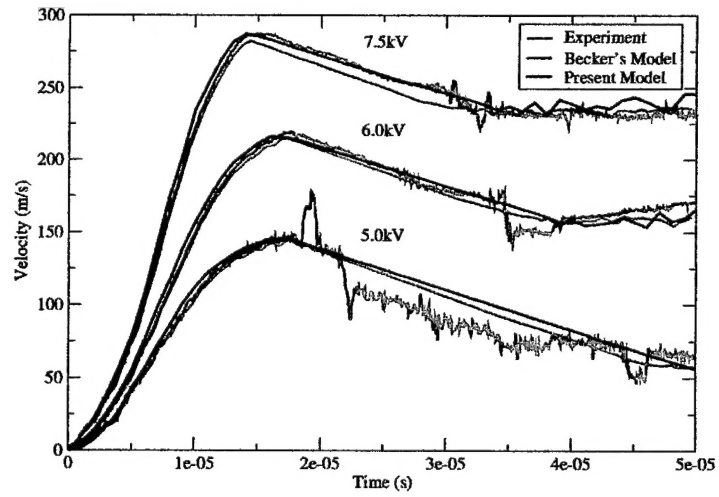Figure 4: Finite element mesh for U-6%Nb rings: 2, 634 nodes, 882 elements.

Figure 5: Velocity history for U-6%Nb rings. Experimental data taken from Becker [1].

Moreover, our results are in excellent agreement with the finite element simulations of Becker [1], despite the considerably coarser discretization of the ring (882 vs. 15,000 elements).
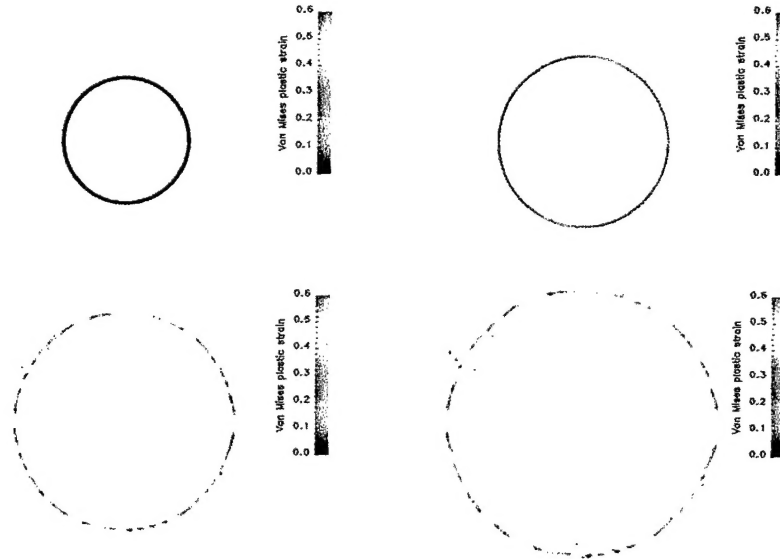

Figure 6: Dynamic fracture and fragmentation of U-6%Nb rings. Configurations at $0\mu s$, $30\mu s$, $60\mu s$ and $90\mu s$.

A sequence of frames of the fracture and fragmentation of the U-6%Nb ring for the 7.5kV applied voltage is shown in Figure 6. The time elapsed between frames is 30 μs, and the color bar is related to the the magnitude of the accumulated plastic strain. For this particular voltage, the time to fracture is approximately 30 μs [1]. The figure clearly shows the expansion of the ring and the process of fracture and fragmentation that begins around 30 μs. The number of major fragments obtained in the simulation is 25, in good agreement with the total of 19 fragments recovered by Becker [1].

6.3   Ballistic Penetration of Mild-Steel Plate - Plugging

The final validation case involves the formation of a shear plug in a circular steel plate subjected to an impact by a blunt -nosed projectile. In the experiments of Borvik *et al.* [2], the projectile launched from a gas gun impacted the center of the target steel plate at 296 m/s. The plate was clamped in a rigid circular frame. The recorded data included the initial and residual velocities at the free end of the projectile.

The formation of shear-bands plays an essential role in the penetration of the target plate by the projectile, as it establishes the clear shear failure path. Should the creation of the shear-bands in the model be constrained, the target plate does not become

8

perforated as the plastic deformation is distributed over larger area.

The target plate has the diameter of 500 mm with the thickness of 10 mm. The length of the projectile is 80 mm and the diameter 20 mm. We model both the target and projectile material as J_2-plasticity mild-steel with thermal updates. The finite element
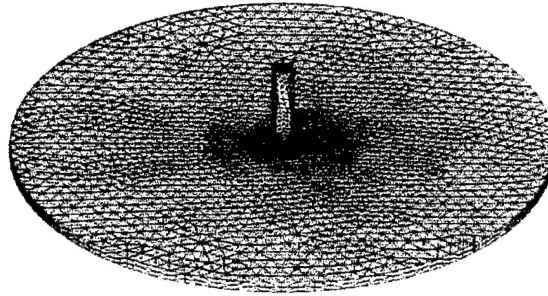

Figure 7: The finite element mesh for ballistic penetration: $11,594$ nodes, $6,430$ elements.

mesh used in our simulations is shown in Figure 7. The initial number of nodes and elements in the mesh is $11,594$ and $6,430$, respectively.

The computed residual projectile velocity at 38.8 μs after the impact is 251.3 m/s, in contrast with the value of 217 m/s reported by Borvik et al. [2]. We attribute the difference to the fact that in the simulations the velocity is recorded at a single node location. However, the average over a set of nodes yields the value of 220.3 m/s, now in very good agreement with the experimental data. In Figure 8 we show a sequence of frames during the perforation of the target plate at $0\mu s$, $33\mu s$, $66\mu s$ and $99\mu s$.

References

[1] R. Becker. Ring fragmentation predictions using the gurson model with material stability conditions as failure criteria. *International Journal of Solids and Structures*, 39(13-14):3555–3580, 2002.

[2] T. Børvik, O.S. Hopperstad, Langseth M., and K.A. Malo. Effect of target thickness in blunt projectile penetration of Weldox 460 E steel plates. *International Journal of Impact Engineering*, 28(4):413–464, 2003.

[3] D.E. Grady and D.A. Benson. Fragmentation of metal rings by electromagnetic loading. *Experimental Mechanics*, 23(4):393–400, 1983.

[4] R. John and S.P. Shah. Mixed-mode fracture of concrete subjected to impact loading. *Journal of Structural Engineering*, 116(3):585–602, 1990.
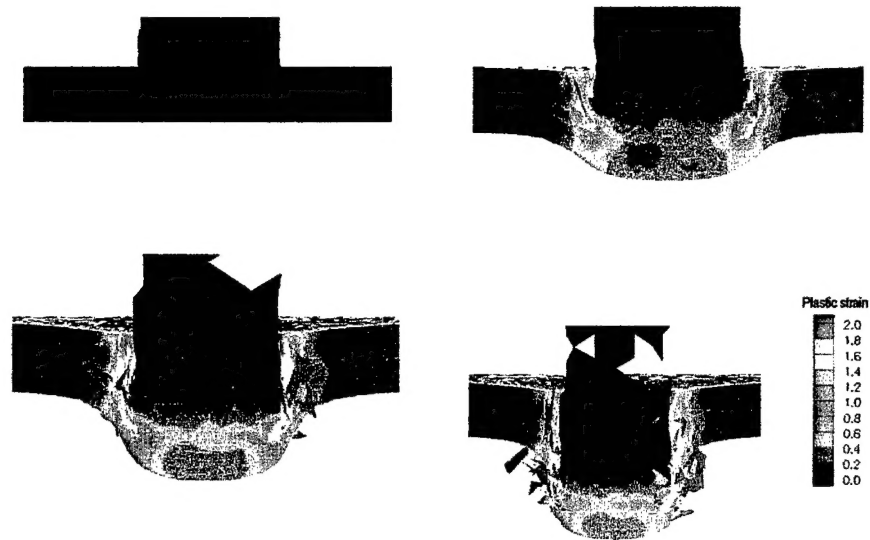
Figure 8: Plugging of mild-steel plate. Configurations at $0\mu s$, $33\mu s$, $66\mu s$ and $99\mu s$.

[5] G. Ruiz, A. Pandolfi, and M. Ortiz. Three-dimensional cohesive modeling of dynamic mixed-mode fracture. *International Journal for Numerical Methods in Engineering*, 52(1–2):97–120, 2001.

[6] P. Thoutireddy, J.F. Molinari, E.A. Repetto, and M. Ortiz. Tetrahedral composite finite elements. *International Journal for Numerical Methods in Engineering*, 53(6):1337–1351, 2002.

[7] K. Weinberg, A. Mota, and M. Ortiz. A variational constitutive model for porous metal plasticity. *Computational Mechanics*, 2004. in preparation.

[8] Q. Yang, A. Mota, and M. Ortiz. A class of variational strain-localization finite elements. *International Journal for Numerical Methods in Engineering*, 2004. submitted.